AIAA JOURNAL
Vol. 33, No. 3, March 1995

Technical Notes

TECHNICAL NOTES are short manuscripts describing new developments or important results of a preliminary nature. These Notes cannot exceed 6 manuscript pages and 3 figures; a page of text may be substituted for a figure and vice versa. After informal review by the editors, they may be published within a few months of the date of receipt. Style requirements are the same as for regular contributions (see inside back cover).

Transonic Wind-Tunnel Flows About a Fully Configured Model of Aircraft

Yoko Takakura*
Tokyo Noko University, Tokyo 184, Japan
and
Satoru Ogawa† and Yasuhiro Wada‡
National Aerospace Laboratory, Tokyo 182, Japan

I. Introduction

In computational fluid dynamics (CFD) for transonic aircraft flows, there is an problem that even the fundamental phases of computed flowfields do not always agree with those in experiments, especially when separation occurs in a large region. Usually flowfields about an object located in a uniform flow are numerically solved and compared, not with flight experiments, but with wind-tunnel experiments. Here, the flowfields in a transonic wind tunnel with a fully configured model of aircraft named ONERA-M5[1] are solved and then compared with wind-tunnel experiments.

Since the beginning of CFD, attempts have been made to solve flows in transonic wind tunnels with perforated test-section walls.[2] In this paper a model is presented to evaluate the outflow or inflow effects through the perforated wall by considering the pressure losses of the fluid and computations of wind-tunnel flows are realized.

The method of numerical analysis used here is summarized as follows.

A. Multidomain Technique

For computations of flows about complex configurations the multidomain technique proposed in Ref. 3 is a very useful and simple method. This technique allows the solution of flowfields on the whole space which is covered with several domains overlapping each other. We use this with a more direct and simpler formulation.[4] For each time step the flow of each domain is independently solved, and then physical values are exchanged between domains by the first-order interpolation scheme. These series of computations proceed until convergence has been reached.

B. Grid Generation

Each grid component is generated independently by an algebraic method where the geometric quantities of a surface are taken into account to generate smooth grids with orthogonality near bodies by marching from the inner to the outer surface.[5] In the multidomain technique, most attention must be given to the grid intervals near the boundary where physical values are exchanged. If the grid intervals of two grid systems differ extremely from each other near that boundary, then transmission of physical information becomes degraded, and at worst the solutions do not converge.

C. Governing Equations and Numerical Scheme

In the individual domain, the three-dimensional thin-layer Navier–Stokes equations in conservation law form are used as the governing equations and are numerically solved by the finite volume method. Space discretization is performed by the Chakravarthy–Osher postprocessing total variation diminishing (TVD) scheme[6] with the improvement that not fluxes but the characteristic variables are extrapolated[7] and that high accuracy is held even at points of extrema.[8] Time integration is executed by the usual first-order explicit method with local time stepping.

The Baldwin–Lomax algebraic turbulence model[9] is used in the individual domain. The intensity of the turbulence of this model is determined using the normal distance from the wall, whereas the normal distance cannot accurately be estimated in the case that the coordinate lines curve and that grids are overlapping. It may be said that the immaturity of the turbulence model becomes evident in solving complex flowfields.

II. Simple Model for Outflow Through Perforated Test-Section Wall

The outflow or inflow effects through the perforated test-section wall of the transonic wind tunnel are modeled with the following considerations.

The perforated wall is considered as an assembly of a circular pipe which has a cross section that reduces and magnifies discontinuously, like Fig. 1. The part with the minimum cross section corresponds to a hole of the wall. Let U_G be the outflow velocity through the wall at a grid point and U_H be the averaged velocity at the hole, when pressure is specified at both sides of the circular pipe: local pressure p is given on the inner side of the test-section wall and constant pressure in the plenum chamber p_{plenum} is on the outer side of that. Usually p_{plenum} is regarded as the uniform-flow pressure p_∞. Let ψ be the porosity ratio.

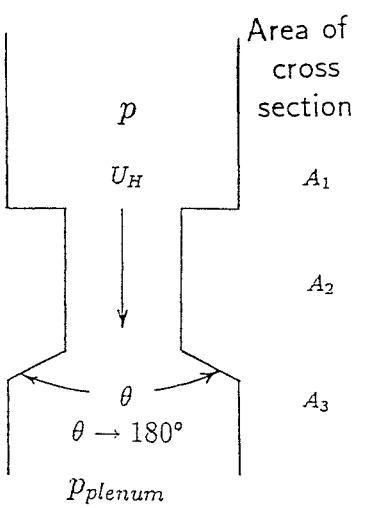

Fig. 1 Modeling for hole on perforated wall.

Presented as Paper 93-3022 at the AIAA 24th Fluid Dynamics Conference, Orlando, FL, July 6–9, 1993; received Aug. 3, 1993; revision received Sept. 6, 1994; accepted for publication Sept. 12, 1994.

*Assistant Professor, Department of Mechanical Engineering, 2-24-16 Nakamachi. Member AIAA.

†Head of Computation Laboratory, Computational Sciences Division, 7-44-1 Jindaiji-Higashi-machi.

‡Senior Researcher, Computational Sciences Division, 7-44-1 Jindaiji-Higashi-machi. Member AIAA.

Then the outflow velocity at a grid point U_G can be described by

$$U_G = \psi U_H$$

The averaged velocity in a hole U_H can be determined by pressure balance

$$p - p_{\text{plenum}} = \Delta p_A + \Delta p_B + \Delta p_C$$

where Δp_A and Δp_B are pressure losses caused by the rapid reduction of cross-sectional area from A_1 to A_2 and magnification from A_2 to A_3, respectively,[10]

$$\Delta p_A = \zeta \rho U_H^2/2, \qquad \zeta = \zeta(A_2/A_1)$$

$$\Delta p_B = \zeta\{1 - (A_2/A_3)\}^2 \rho U_H^2/2, \qquad \zeta = \zeta(\theta)$$

$$\theta \to 180 \text{ deg}$$

and Δp_C is a pressure loss caused by the frictional drag in the hole, which is negligible compared with the two losses.

III. Computational Results and Discussion

A. Computational Grids and Numerical Condition

As shown in Fig. 2, the computational region covers the whole part of the test section and squared diffuser of the wind tunnel with five domains: wind-tunnel, fuselage and sting (body-sting), main wing, horizontal-tail (h-tail) wing, and vertical-tail (v-tail) wing domains, D_1, D_2, D_3, D_4 and D_5 ($D_1 \supset D_2$, $D_2 \supset D_3$, $D_2 \supset D_4$, $D_2 \supset D_5$). The number of grid points on each grid system is shown in Table 1.

Table 1 Number of grid points on each grid system

Domain	Kind of domain	Grid-point number[a]
D_1 : wind-tunnel	Main	121 × 45 × 31
D_2 : body-sting	Submain	131 × 69 × 37
D_3 : main wing	Sub	121 × 45 × 31
D_4 : h-tail wing	Sub	93 × 31 × 21
D_5 : v-tail wing	Sub	61 × 35 × 21

[a]In order of streamwise, circumferential/spanwise, and normal directions.

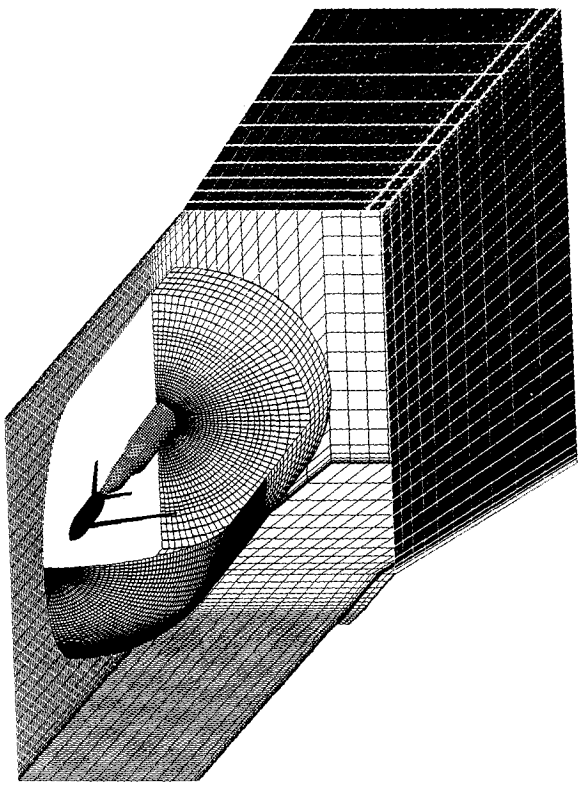

Fig. 2 Whole grid view for test section and squared diffuser of wind tunnel.

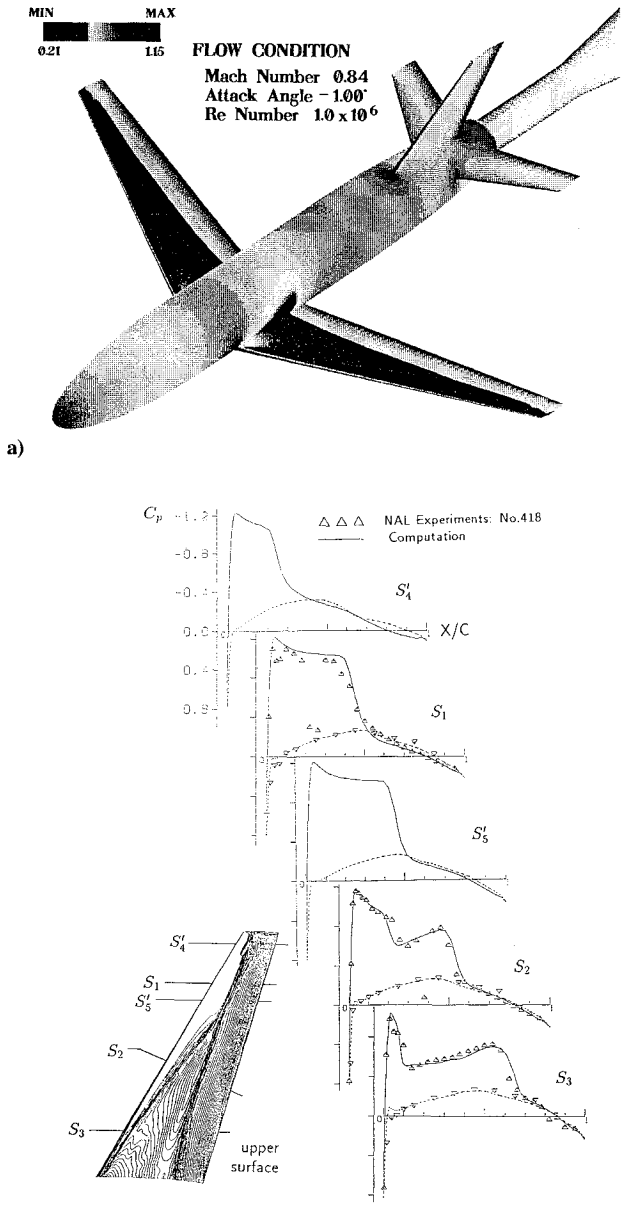

Fig. 3 Numerical solution on ONERA-M5 model $M_\infty = 0.84, Re = 10^6, \alpha = -1$ deg: a) pressure distribution and b) C_p distributions on main wing.

To avoid smearing numerical solutions when exchanging physical quantities near the attached region of the fuselage and each wing, each subdomain of the wing is fitted not only to the wing surface but also to the fuselage surface in each grid system. The minimum grid size at the wall is taken as 10^{-4} of the mean chord length of the main wing.

Flows about the ONERA-M5 aircraft model within the National Aerospace Laboratory (NAL) transonic wind tunnel are numerically solved under the flow condition of Mach number 0.84 and Reynolds number based on the mean chord length of the main wing, 10^6.

B. Case for $\alpha = -1$ deg

When the attack angle for the fuselage is −1 deg, that for the main wing is about 3 deg because the incidence angle is about 4 deg. Figures 3a and 3b show distributions of pressure on the aircraft and pressure coefficients on the main wing, respectively. In this figure the triple shock wave (weak and strong shock waves and their united shock wave) is clearly observed on the main wing, and that agrees well with NAL experimental data (No. 418). Investigating the solution near the connection of fuselage edge and sting, C_p takes negative values at the rear edge of the fuselage and positive values at

Table 2 Comparison of C_L and C_D vs α between computations and experiments

		$\alpha = -1$ deg	$\alpha = -2$ deg	$\alpha = -3$ deg
C_L	Computations	0.268	0.120	−0.0151
	Experiments	0.259	0.130	0.0201
C_D	Computations	0.0259	0.0215	0.0205
	Experiments	0.0266	0.0213	0.0198

the root of sting. Perhaps separation is caused by the step between the fuselage edge and the sting, and this phenomenon strongly affects the calculation of drag. Both the lift and drag coefficients agree well with experimental data (see Table 2).

C. Cases for Series of Attack Angles

Table 2 shows the values of lift and drag coefficients for $\alpha = -1, -2$, and -3 deg. Except for the lift for $\alpha = -3$ deg, both the lift and drag coefficients agree well with experiments. It is especially remarkable that the computed drag corresponds well with wind-tunnel experiments, since, typically, in computations of aircraft flows the drag does not compare with the data.

IV. Concluding Remarks

The transonic flows about a fully configured model of aircraft named ONERA-M5 within the NAL transonic wind tunnel have been numerically solved to investigate the reliability of numerical solutions. The multidomain technique was used to solve the whole flowfield around the complicated configuration. In each domain the grid was generated by an algebraic method and the thin-layer Navier–Stokes equations were solved by the improved Chakravarthy–Osher TVD scheme. Further, a simple model was presented to estimate the outflow/inflow effects at the perforated wall of the transonic wind tunnel. The results obtained by the present methods have shown good coincidence with the experimental data of NAL wind-tunnel test, in regard to local C_p distributions on the main wing and total forces C_L and C_D.

Therefore, in spite of the primitive model for the perforated wind-tunnel wall and the immature algebraic turbulence model, we believe that this numerical analysis is the first step for the more precise evaluation of the numerical solutions and wind-tunnel experiments.

References

[1]Anon., "Experimental Data Base for Computer Program Assessment, Report of the Fluid Dynamics Panel Working Group 04," AGARD Rept. AR-138, 1979.

[2]Baldwin, B. S., Turner, J. B., and Knechtel, E. D., "Wall Interference in Wind Tunnels with Slotted and Porous Boundaries at Subsonic Speeds," NACA TN-3176, May 1954.

[3]Benek, J. A., Buning, P. G., and Steger, J. L., "A 3-D Grid Embedding Technique," AIAA Paper 85-1523, July 1985.

[4]Takakura, Y., and Ogawa, S., "Computations of Transonic Flows about a Fully Configured Model of Aircraft Using a Multi-Domain Technique," *Computers and Fluids* (to be published).

[5]Takakura, Y., and Ogawa, S., "A Simple Grid Generation Technique for Hypersonic Flow Around Complex Configuration," *Proceedings of the 9th NAL Symposium on Aircraft Computational Aerodynamics*, National Aerospace Lab. SP-16, Tokyo, Dec. 1991, pp. 9–14.

[6]Chakravarthy, S. R., and Osher, S., "A New Class of High Accuracy TVD Schemes for Hyperbolic Conservation Laws," AIAA Paper 85-0363, Jan. 1985.

[7]Takakura, Y., Ishiguro, T., and Ogawa, S., "On TVD Difference Schemes for the Three-Dimensional Euler Equations in General Coordinates," *International Journal for Numerical Methods in Fluids*, Vol. 9, No. 8, 1989, pp. 1011–1024.

[8]Wada, Y., Kubota, H., Ogawa, S., and Ishiguro, T., "A Diagonalizing Formulation of General Real Gas-Dynamic Matrices with a New Class of TVD Schemes," AIAA Paper 88-3596-CP, July 1988.

[9]Baldwin, B. S., and Lomax, H., "Thin Layer Approximation and Algebraic Model for Separated Turbulent Flows," AIAA Paper 78-257, Jan. 1978.

[10]Anon., "Fluid Motion," *Kagaku Kogaku Binran*, 5th ed., Kagaku Kogaku Kyokai, Tokyo, 1988, pp. 262–263.

Experimental Study of Perturbed Laminar Wall Jet

C. Shih* and S. Gogineni†
Florida A&M University and Florida State University, Tallahassee, Florida 32316

Introduction

A PLANE wall jet is a stream of fluid blown tangentially along a plane wall. It has a wide range of applications, such as boundary-layer control over a wing, film cooling on turbine blades, etc. It consists of two distinct regions: 1) an outer shear layer that is subjected to the inviscid Kelvin-Helmholtz instability and 2) an inner layer that behaves like a viscous boundary layer. The interaction between the structures from these two layers leads to the eventual laminar to turbulent transition. Katz et. al.[1] observed that the external excitation on the plane turbulent wall jet has no appreciable effect on either the maximum velocity decay or the spreading rate of the jet. The linear stability calculations by Cohen et. al.[2] indicated the existence of two unstable modes: an inviscid mode that represents the large-scale disturbances in the free shear layer, plus a viscous mode describing the small-scale disturbances near the wall. They have also shown that the relative importance of each mode can be controlled by subjecting the wall jet to small amounts of blowing or suction. The extensive literature available on wall jets is mainly based on either pointwise measurements, flow visualization studies, or analytical/numerical investigations. However, to understand the unsteady flow characteristics associated with the dynamic behavior of the vortices and their interactions, it is necessary to study the spatial vorticity distribution at each instant. In view of this, we proposed to examine the flowfield using particle image velocimetry (PIV). This technique can provide the instantaneous two-dimensional velocity data in a selected plane of the flowfield with sufficient spatial accuracy such that the instantaneous vorticity field can be obtained. For a detailed description of the PIV technique, please refer to Adrian[3] and Lourenco et al.[4]

The focus of the present investigation is to describe the effects of using a low-frequency, high-amplitude external acoustic excitation on a wall jet and the subsequent interactions between the inner and outer region vortical structures. Both PIV and smoke/laser sheet flow visualization techniques are used for the understanding of the global dynamics of the interaction process.

Experimental Setup

The experimental facility is shown schematically in Fig. 1. The wall jet originates from a two-dimensional channel ($h \times W \times L = 0.5 \times 10.0 \times 52.7$ cm) that is connected to a settling chamber via a two-stage contraction. The aspect ratio of the nozzle (W/h) is 20. Because of the long developing length of the channel ($L/h = 105.4$), the exit velocity profile is a fully developed parabolic profile. A loudspeaker attached to the settling chamber is used to perturb acoustically the wall jet (Fig. 1). The wall is made of Plexiglas plate with side walls to minimize the influence of the side edges. The jet is seeded with smoke particles produced by a Rosco-type 1500 smoke generator. The entire apparatus is placed inside an enclosure (1.5×1.5 m in cross section) with three sides covered by plastic sheets to minimize the outside influence. A second smoke generator of the same type is used to seed the outside ambient flow surrounding the jet. A Cartesian coordinate system (x, y, z) is chosen as shown in Fig. 1. A dual pulsed laser system consisting of two Spectra-Physics DCR-11 Nd:YAG pulsed lasers is used to provide the double illumi-

Received Aug. 22, 1994; revision received Oct. 10, 1994; accepted for publication Oct. 15, 1994.

*Associate Professor, Department of Mechanical Engineering, College of Engineering. Member AIAA.

†Research Assistant, Department of Mechanical Engineering, College of Engineering; currently NRC Postdoctoral Fellow, Aero Propulsion and Power Directorate, Wright Patterson AFB, OH 45433. Member AIAA.